X-RAY INTENSITY, OZONE DENSITY, AND VLF WAVE INTENSITY OBSERVED BY SCIENTIFIC BALLOON EXPERIMENTS AT ESRANGE

Masaki EJIRI, Masaru AYUKAWA, Hisao YAMAGISHI,
Takayuki ONO, Takeo HIRASAWA,

National Institute of Polar Research, 9–10, Kaga 1-chome, Itabashi-ku, Tokyo 173

Tetsuo KAMADA,

*Research Institute of Atmospherics, Nagoya University,
13, Honohara 3-chome, Toyokawa 442*

Masahiro KODAMA,

*Yamanashi Medical College, Tamaho-mura,
Nakakoma-gun, Yamanashi 409-38*

Yo HIRASIMA,

Rikkyo University, 34–1, Nishi-ikebukuro 3-chome, Toshima-ku, Tokyo 171

Toshihiro OGAWA, Naomoto IWAGAMI

University of Tokyo, 3–1, Hongo 7-chome, Bunkyo-ku, Tokyo 113

and

Takamasa YAMAGAMI

*The Institute of Space and Astronautical Science,
6–1, Komaba 4-chome, Meguro-ku, Tokyo 153*

Abstract: The first Japanese scientific balloon experiment at Esrange, Kiruna, Sweden was carried out on September 10 and 11, 1980, in order to obtain vertical profiles of X-ray intensity, ozone density, and VLF wave spectrum intensity at a northern high-latitude. Since there were very quiet geomagnetic conditions for two balloon flights, observational results reveal a typical quiet time X-ray intensity profile and an ozone vertical profile in the high-latitude autumn. No evident VLF emissions associated with an auroral activity were observed, except for noises of power line radiation and lightning noises from Africa. Ground-based observations of the three components of geomagnetic field, cosmic noise absorption, pulsations and VLF waves were made in conjunction with the one month campaign and the data corresponding to several substorms were analyzed and compared with observations at the Syowa Station, Antarctica.

1. Introduction

During the past two decades the scientific balloon experiment has been developed as one of the powerful observational techniques to study the high-latitude upper atmo-

155

spheric phenomena.   For example, ROSENBERG *et al.* (1981) revealed a close correlation of electron bursts and VLF chorus associated with magnetospheric substorms with high-latitude balloon observations.   There have been also many balloon experiments performed at Syowa Station, Antarctica.   For example, through their experiments, KODAMA *et al.* (1972) discussed auroral X-rays and their conjugacies between Southern and Northern Hemispheres.

Auroral X-rays present evidence for precipitations of auroral particles, especially energetic electrons.   The purpose of balloon observations is being changed from a morphological study based on the intensity-time profile of X-rays into a fine structure measurement of spatial distribution and dynamics from a three-dimensional viewpoint.   The former is mainly limited to the observations by means of a single balloon at one location (*e.g.*, WINCKLER *et al.*, 1958), while the latter comprises simultaneous observations using multiple balloons (*e.g.*, BARCUS *et al.*, 1973), or using the X-ray imaging (camera) technique (MAUK *et al.*, 1981).   YAMAGAMI *et al.* (1978) determined auroral illuminating regions for active auroral X-ray burst events, using three sets of NaI (TI) scientillation counters, and showed a constant inflow of auroral X-rays from a specific direction with an interval of 2 min.   The satellite observation of auroral X-ray images by IMHOF *et al.* (1980) attained a 65 km spatial resolution, while the balloon observations by MAUK *et al.* (1981) have revealed smaller scale (less than about 15 km) spatial structures.

As for the ozone density, its world-wide distribution has been studied extensively since the International Geophysical Year, 1957–1958, and it has been measured recently by using the satellites such as Nimbus (*e.g.*, HILSENRATH *et al.*, 1979).   Several observational and theoretical studies (*e.g.*, NICOLET, 1975; CHANDRA and MAEDA, 1980; HILSENRATH, 1980) have been developed for the dynamical behavior of the stratospheric ozone in the polar region at times of occurrence of auroral activities, cosmic rays, and during the polar night; however there have been no conclusive results presented so far.

Though considerable ground-based observations have been made on ULF, ELF and VLF wave phenomena associated with polar disturbances and directly connected to the auroral phenomena (*e. g.*, SATO, 1980), many are still under investigation both phenomenologically and theoretically.

The first Japanese scientific balloon experiment was carried out on September 10 and 11, 1980, at Esrange (62°52.2′N and 21°04.2′E), Kiruna, Sweden, in order to make observations of X-ray intensity, ozone and VLF wave spectrum intensity at the northern high-latitude (auroral zone).   The paper describes the results of two balloon flights, together with ground-based observations of the three components of geomagnetic field, cosmic noise absorption, pulsations and VLF waves made during this campaign.

2.   Instrumentation

Two identical sets of scientific balloons were constructed as shown in Fig. 1; the main balloon was a Japanese manufactured 5000 m³ type B-5 and the auxiliary balloon was a French Zodiac 60 m³ type 1/8 AX P50.   An outline and the results of this campaign were given by AYUKAWA and EJIRI (1980).   Following are brief de-
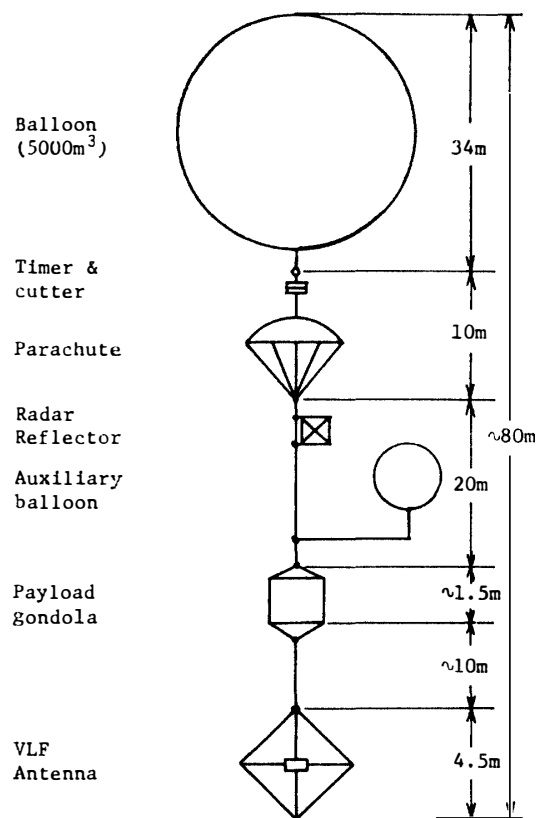
Fig. 1. Sounding balloon flight train.

scriptions of the scientific payloads onboard.

2.1. X-ray detector

Auroral X-ray observations planned as a part of the project had been aimed to measure the spatial distribution with better accuracy as possible by using a currently developed technique of a multi-plate image intensifier. Since in practice it is better to proceed step by step, the first two flights were tried with the simplest design of payload. The X-ray sensor consists of a NaI (TI) type 4×20 scintillator ($1'\phi \times 2$ mm), a photo-multiplier type 6199 and a collimator with a 90° field of view (full) being directed toward the zenith. The energy range of measured X-rays is from 20 keV to 150 keV.

2.2. Ozone detector

Ozone density, atmospheric temperature and pressure were measured by the standard electrochemical ozone-sonde RSII-KC79, fabricated by Meisei Denki Co., Ltd. and used routinely by the Japan Meteorological Agency, which was slightly modified to adapt it to this particular flight. Because of the long flight time, an extra tank for the potassium iodide sensing solution was added. A minor modification of the pressure sensor was made in order to measure an atmospheric pressure variation during the balloon ceiling flight. For the characteristics of this ozone-sonde, see KOBAYASHI and TOYAMA (1966).
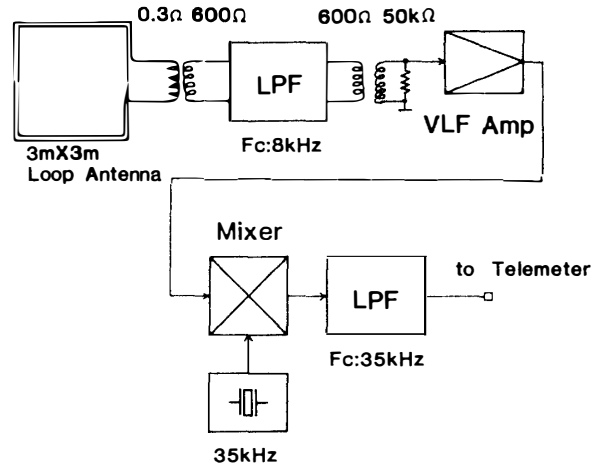
Fig. 2. Block-diagram of VLF wave detector system.

2.3. VLF wave detector

The block diagram of the system is illustrated in Fig. 2. The sensor, being located at 10 m away from the other instruments installed in the gondola (see Fig. 1), is a diamond-shape 2-turn loop antenna (3 m × 3 m) with a resistance of 0.20Ω, an inductance of 66.2 μH and an effective height of $5.14 \times 10^{-4} \times f$ in meters, where f is a receiving frequency in kHz. Omega signals are eliminated at the input pre-amplifier and the equivalent power flux of the receiver noise level is 3.1×10^{-15} W/m$^2 \cdot$Hz at 1 kHz. The received wide band signals are transmitted to the ground by VSB modulation telemetry with a sub-carrier frequency of 35 kHz. The ground telemetry demodulator gives a signal from 0.2 kHz to 8 kHz.

2.4. Ground-based equipments

A VLF wave detector and an induction magnetometer for the ground-based observations of this campaign were specially designed and fabricated. The VLF sensor is a 1-turn loop antenna 10 m in height and 45 m in circumference, with a resistance of 0.08Ω, an inductance of 68.8 μH and an effective height of $2.58 \times 10^{-3} \times f$ in meters where f is the receiving frequency in kHz. The input pre-amplifier has a constant resistance network with an input step-up transformer of 0.3Ω: 600Ω, as shown in Fig.
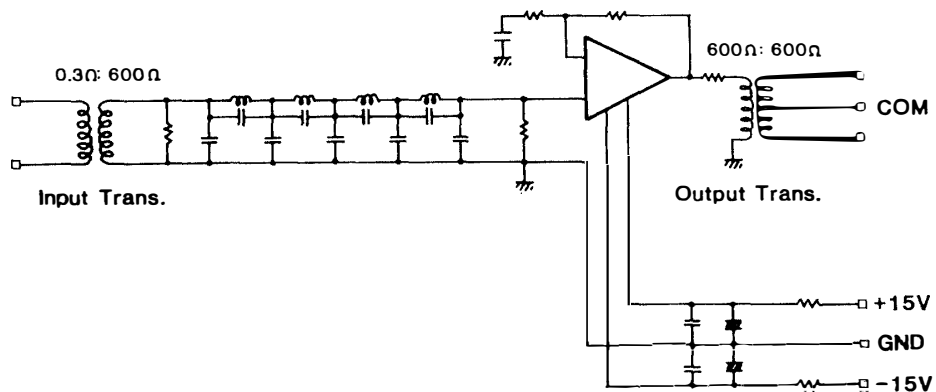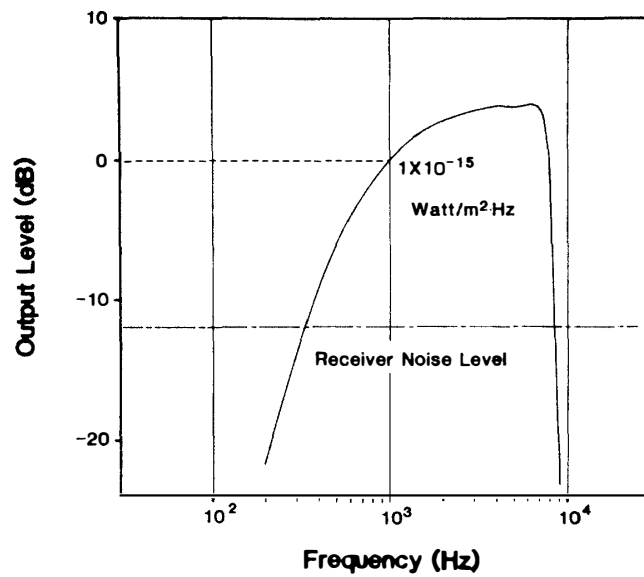

Fig. 3. VLF receiver pre-amplifier.

Fig. 4. *Frequency characteristics of the output voltage of the ground-based VLF wave receiver system.*
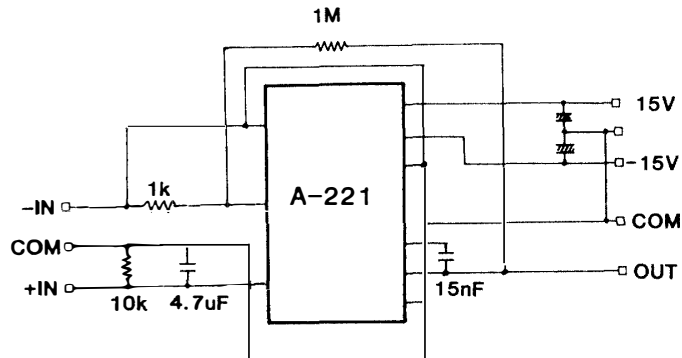

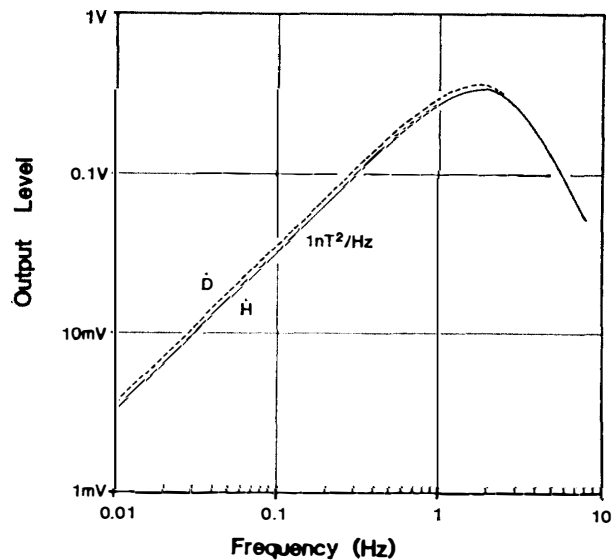*Fig. 5.* *Input amplifier of the induction magnetometer.*

Fig. 6. *Frequency characteristics of the induction magnetometer.*

3. Omega signals are eliminated by the filter. The frequency characteristics of the output voltage of the system including a main amplifier is depicted in Fig. 4, where 0 dB is equal to 6.05×10^{-4} Vrms/$\sqrt{Hz}$ equivalent to 1×10^{-15} W/m²·Hz at 1 kHz. The receiver noise level is 6.3×10^{-17} W/m²·Hz at 1 kHz.

The induction magnetometer has a sensor using a laminated Permalloy strip core with a cross-section area of 1 cm² and a length of 75 cm. The coil is 10^5-turns of 0.2 mm diameter enamel wire with a resistance of 4.2 kΩ and an inductance of 1.5 kilohenry, a 20-turns calibration coil of 0.39Ω. The effective cross-section area for the $\dot{H}$ sensor is 8.4×10^3 m² and that for $\dot{D}$ sensor 9.4×10^3 m². The input amplifier illustrated in Fig. 5, adopts a chopper-type amplifier which prevents the DC output level from drifting and has a low signal to noise ratio. The frequency characteristics of the system is depicted in Fig. 6; the ordinate is in RMS volts. The equivalent power flux of the sensor noise level is $4.0 \times 10^{-5} \gamma^2$/Hz at 1 Hz.

3. Experimental Results and Discussions

Two scientific balloons were launched at 1744 LT on September 10 and 1918 LT on September 11, 1980, with ceiling floating periods of about 1 h 38 min and 1 h 24 min, respectively. Geomagnetic conditions for these days were very quiet, ΣKp being 9 and 13−, and were identified as quiet days as listed in the Geomagnetic and Solar Data, WDC-A for STP, NOAA, Boulder. Balloon trajectories for the two flights are shown in Fig. 7. Note that the actual altitude of the balloon which was determined by radar is used in the following figures.
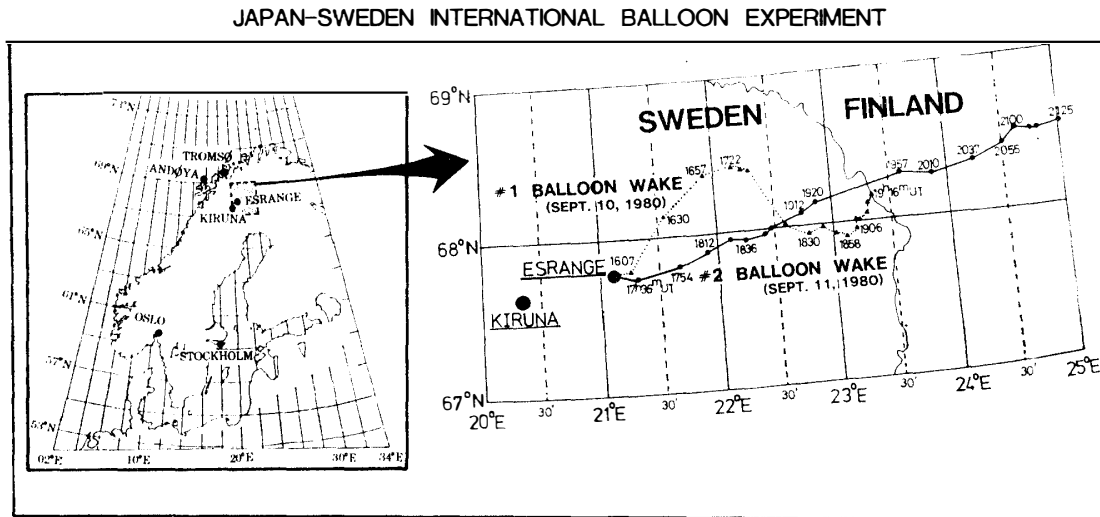
JAPAN–SWEDEN INTERNATIONAL BALLOON EXPERIMENT

Fig. 7. Balloon trajectories for two flights, #1 and #2.

3.1. X-ray intensity

Observational results from the two flights show a typical height profile of background X-rays along both ascending and descending flight passes, with a maximum counting rate around the Pfotzer maximum of about 17 to 18 km in height, as shown in Figs. 8a and 8b. Counting rates of the X-ray intensity at the balloon ceiling al-
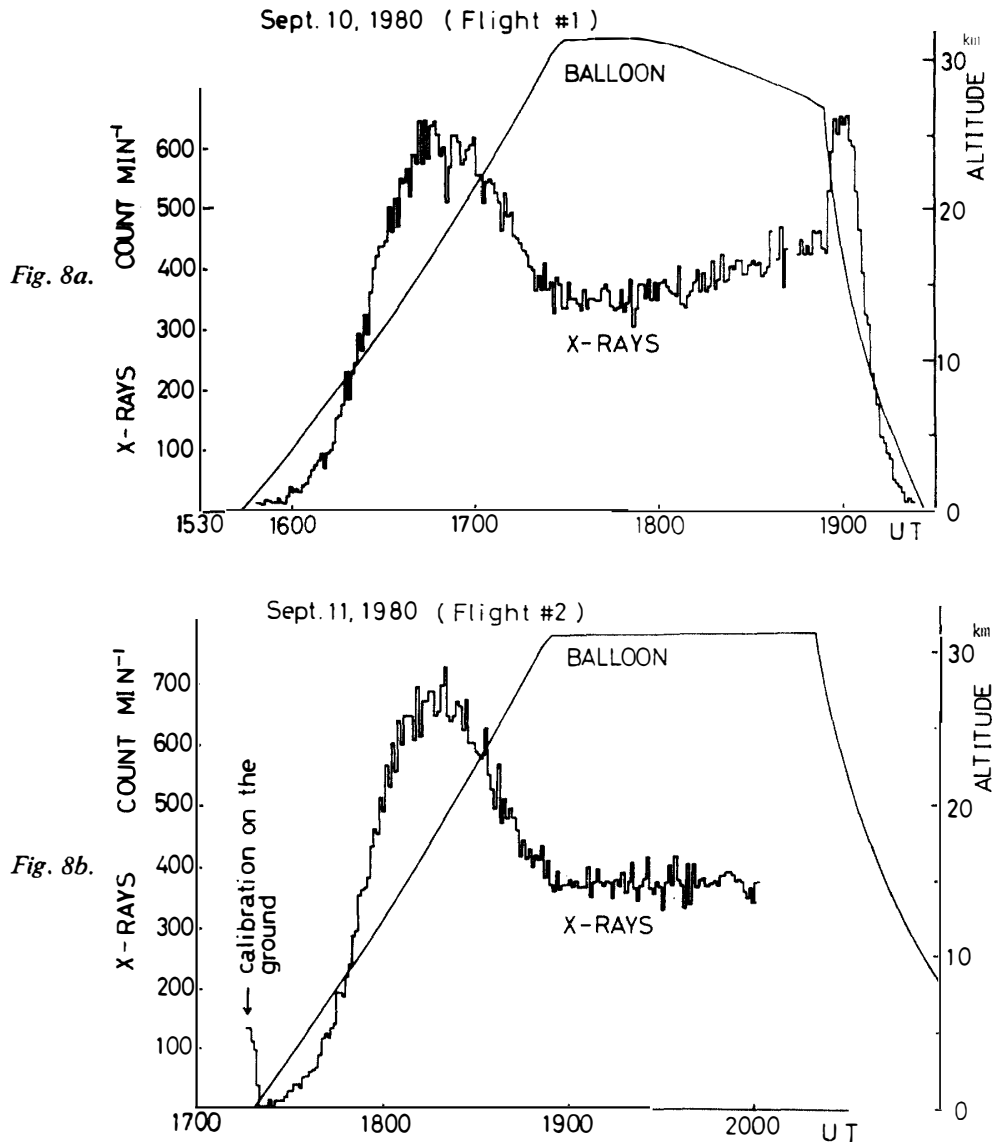
Fig. 8. *X-ray counting rates observed with (a) #1 balloon payload on September 10, 1980 and (b) #2 balloon payload on September 11, 1980, at Esrange. The balloon flight curve is also shown.*

titude of 10 mb were kept constant, being 5.8/s and 6.3/s for #1 and #2 flights, respectively. Taking into account the geometrical parameters of the detector, the background X-ray fluxes in the energy range 20–150 keV are $1.7/cm^2 \cdot s \cdot sr$ and $1.9/cm^2 \, s \cdot sr$ respectively. These give a value corresponding to a quiet geomagnetic condition at the high latitude. Discussions about their reliability will follow.

In general, there is little contribution of either the diffuse cosmic X-rays of bremsstrahlung X-rays emitted by the interaction of cosmic ray electrons with the payload materials to the X-rays background observed at the balloon altitude. Most of the X-rays background is explained by the atmospheric component of cosmic rays. In other words, the background X-ray flux is mainly subject to the latitude and altitude dependences of cosmic ray intensity.

According to the balloon observations by YAMAGAMI *et al.* (1978) at Thompson (55.8°N, 262.1°E), the background X-ray flux in the energy range 15–85 keV measured at a depth of 6 gcm^{-2} was 2.5/cm^2·s·sr. A similar experiment made at a smaller depth of 3.5 gcm^{-2} gave 1.6/cm^2·s·sr for the same energy range at 40°N geomagnetic latitude (PETERSON, 1969). The expected flux at Esrange, estimated from the above experimental values, is about 2.0/cm^2·s·sr, assuming a difference of 5 keV in the lower threshold energy, altitude and latitude dependences of total cosmic ray flux. Therefore, the presently observed flux values are consistent with those to be expected.

3.2. Ozone density

Height profiles of the ozone density were obtained during two sounding balloon flights, except for the regions above 15 km along the descending pass of #1 flight (September 10) and the regions above 13 km along the ascending pass of #2 flight (September 11). Atmospheric temperature and pressure were measured, except along the descending pass of #2 flight due to the low signal to noise ratio of the telemetry channel. Figures 9, 10 and 11 illustrate the above results, together with atmospheric temperature and pressure profiles of the U.S. Standard Atmosphere.

The observed ozone height-profile reveals a sudden increase in density above the tropopause (~9.6 km) with a maximum around an altitude of 20 km, which is the typical profile of ozone density in autumn at high-latitudes. The total ozone content for this profile is calculated to be 5.6×10^{18} cm^{-2} (or 0.21 atm-cm) which is a little lower value than normal, even taking into account of the fact that the ozone content in the Northern Hemisphere has a minimum value in September.

The observed atmospheric temperature profile seems to be real even though there are several degrees of deviation (10°C at most) from the U.S. Standard Atmosphere. On the other hand the observed atmospheric pressure indicates an error in the measur-
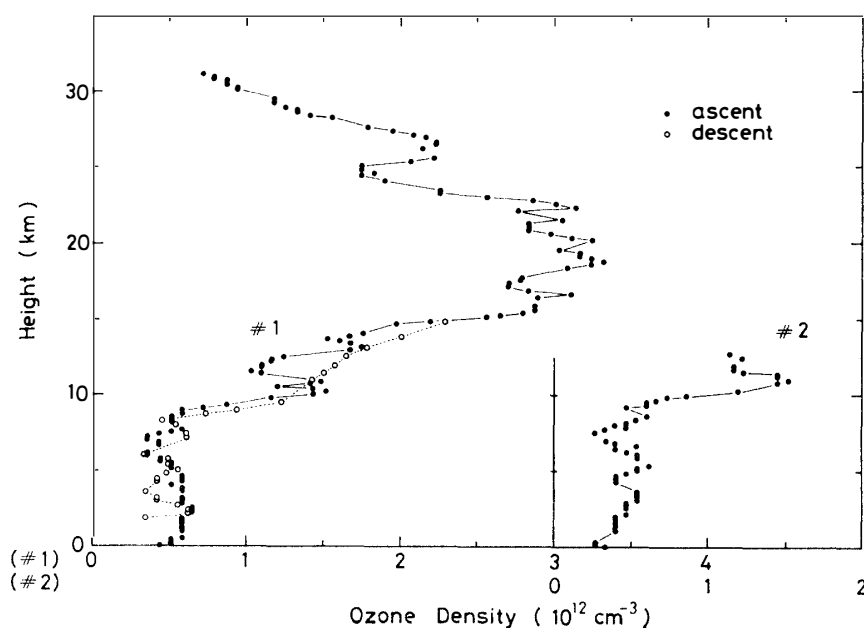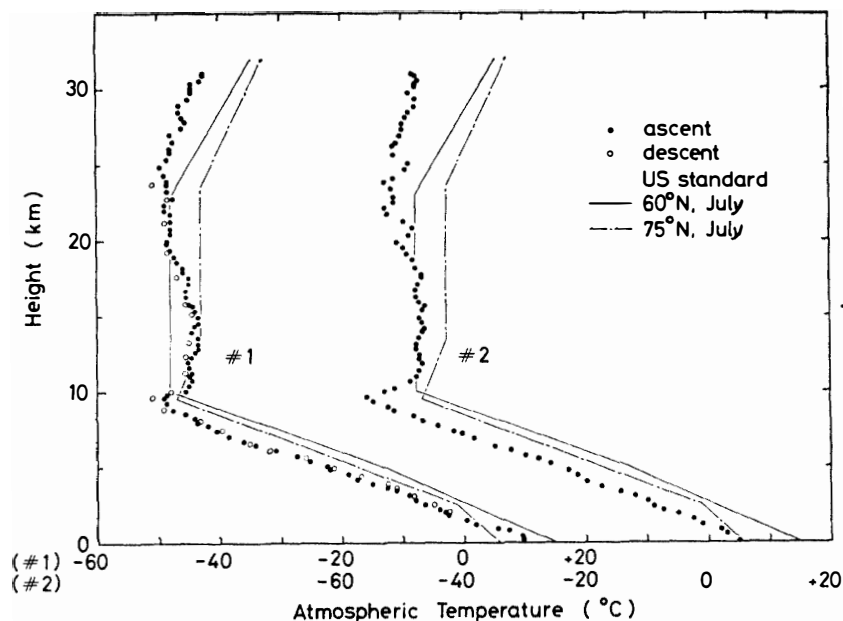

Fig. 9.   Observed ozone density profiles.

Fig. 10. Observed atmospheric temperature profiles. Also shown are the values of U.S. Standard Atmosphere (60°N and 75°N, July).
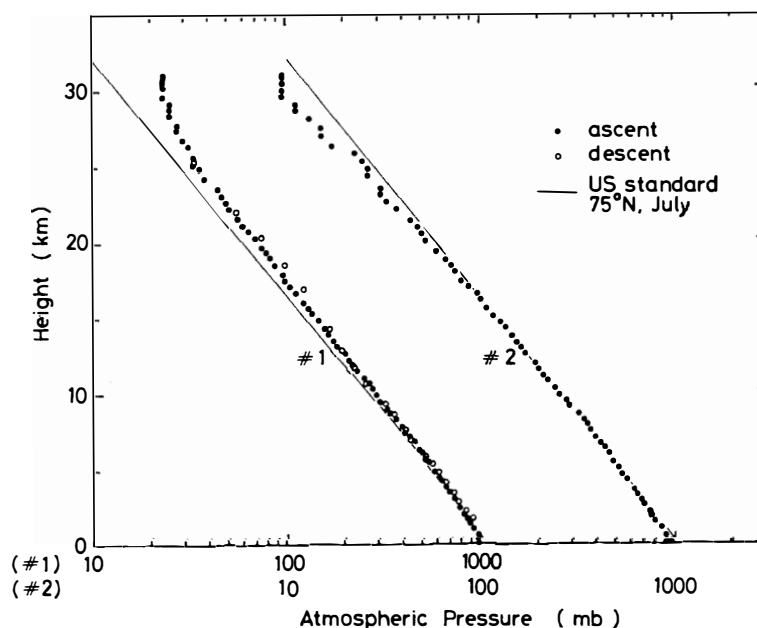

Fig. 11. Observed atmospheric pressure profiles. Also shown are the values of U.S. Standard Atmosphere (75°N, July).

ing system because of the large deviation from the U.S. Standard Atmosphere at higher altitudes.

3.3. VLF wave intensity

Since the geomagnetic conditions for these two flights were quiet, no significant VLF emissions associated with polar disturbances were observed. However, other

kinds of VLF noises were observed, and identified as the higher harmonics of power line radiation (PLR) and waveguide propagation of atmospheric noise originating from lightning in Africa.

3.3.1. Higher harmonics of power line radiation (PLR)

VLF wide band data demodulated through the telemetry system are analyzed with the FFT analyzer (1024 data points a resolution of 2.5 Hz and an analyzed interval of 6.5 ms). Then, intensity profiles of 5th and 9th harmonics, *i.e.* 250 Hz and 450 Hz respectively, are plotted against balloon flight time during the ascending pass. Figure 12 shows the results for both flights. Variations of signal intensities over 20 dB with a period of 10 s to 60 s and their obvious directivity patterns due to rotational motion of the antenna suggest that the magnetic field vector of PLR higher harmonics is a uniformly polarized vector in the horizontal plane, and the harmonic radiations are coherent.

The time variation of the envelopes of peak intensities are also shown in the figure, and that for #1 flight is smaller than that for #2 flight. This result is consistent with the fact that #1 payload moved away from the launching point more slowly than #2
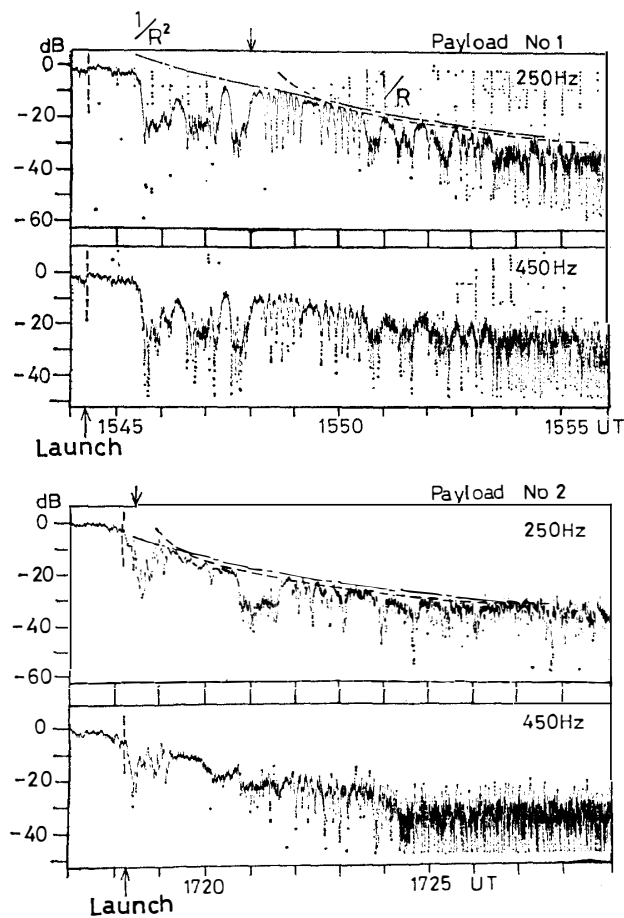

Fig. 12. Intensity variations of harmonics of power line radiations for #1 (upper panel) and #2 (lower panel) payloads.
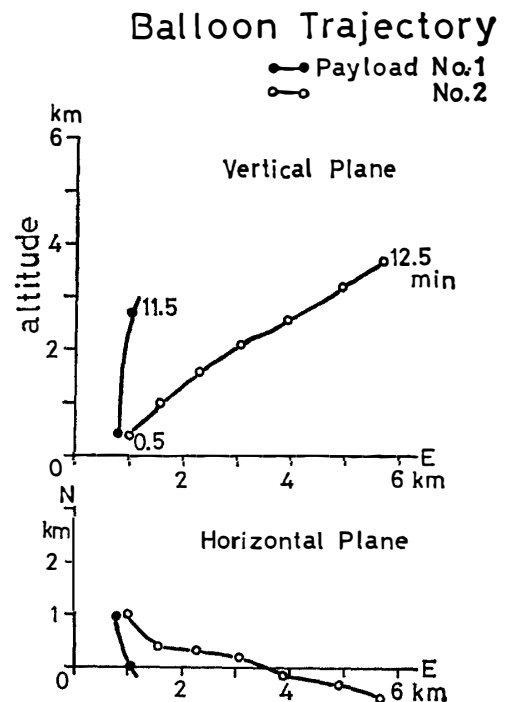
Fig. 13. Balloon trajectories near the launching pad.

payload, as is clearly illustrated in Fig. 13.   Since PRL sources are presumably localized around the Esrange facility area and along the route of the power lines coming into the range, the variation of the envelope should vary as R^{-1} or R^{-2} where R is the distance between the launching pad and the balloon, depending on whether the source is a point source or a line source.   If a point source is assumed, the interpolated location for an envelope varying as R^{-1} indicates a source marked by the arrow on top portion of each panel of Fig. 12.

3.3.2.   Height profile of atmospheric noise

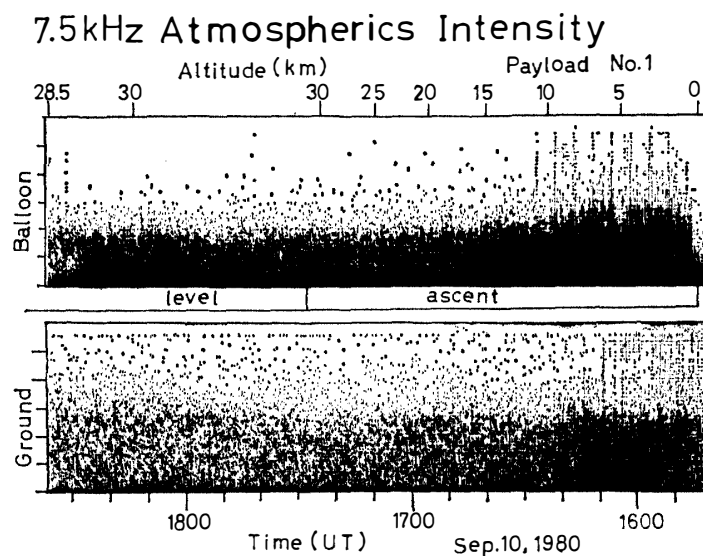VLF wide band data are analyzed by the FFT analyzer, and the peak intensity

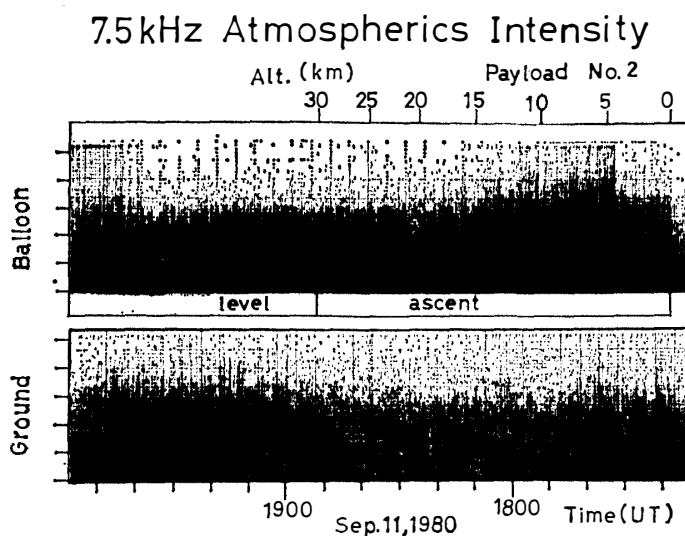Fig. 14.   7.5 kHz atmospherics intensity observed with #1 payload in flight and on the ground.

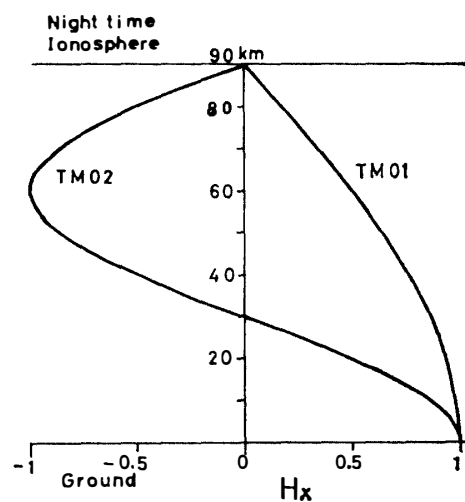Fig. 15.   7.5 kHz atmospherics intensity observed with #2 payload in flight and on the ground.

Fig. 16.   Schematical diagram of intensities of H-component for VLF wave-guide propagation modes TM01 and TM02.

of 7 kHz components for 6 s (equal to 1/2 spin period of an antenna) is recorded. The same processes are applied to the ground-based VLF observational data for comparison, with results as shown in Figs. 14 and 15 for the ascents of payloads #1 and #2, respectively. For both cases of the flight data, the atmospheric noise increases rapidly right after the lift-off and then decreases with the increase of the balloon height. There are no such changes in intensity in the ground-based data. The lightning source for this noise is most likely located in Africa, the noise signals propagate by a waveguide mode (WAIT, 1962); probably by the TM01 and TM02 modes at night time as schematically illustrated in Fig. 16. The observed noise intensity profiles show changes consistent with this result, *i.e.* a monotonic decrease with height.

3.4. Ground-based observations

Table 1 is a list identifying the periods, during which significant VLF emissions associated with auroral activities were observed on the ground. Two events, *i.e.*

Table 1. Observed periods of VLF emission.

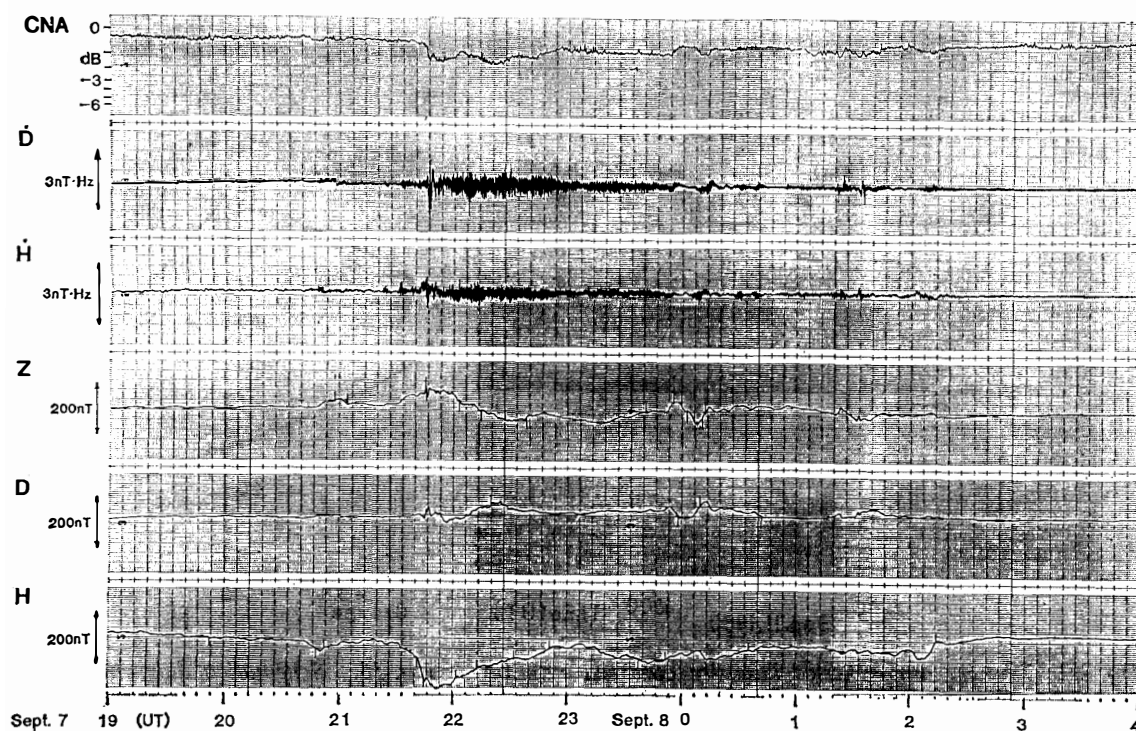| Sept.	6	0625–0655		Sept.	13	0310–0330
Sept.	7	2316–2317				0600–1020
		2333–2345				1900–2400
Sept.	8	0028–0130		Sept.	14	0000–0250
		0207–0213				0500–0700
Sept.	12	0235–0325		Sept.	15	2250–2300
		0440–0600				

Fig. 17.   September 7 event; ground-based observations.

September 7 to 8 and September 13 to 14, are discussed in detail.

3.4.1. September 7 event

Between September 7, 19 UT and September 8, 04 UT, there were geomagnetic substorms with a negative bay of about 200 nT and -1 dB CNA occurring at 2151 UT. The recorded data for CNA, pulsations and the 3-components of geomagnetic field are depicted in Fig. 17. There was an active aurora borealis display in the sky
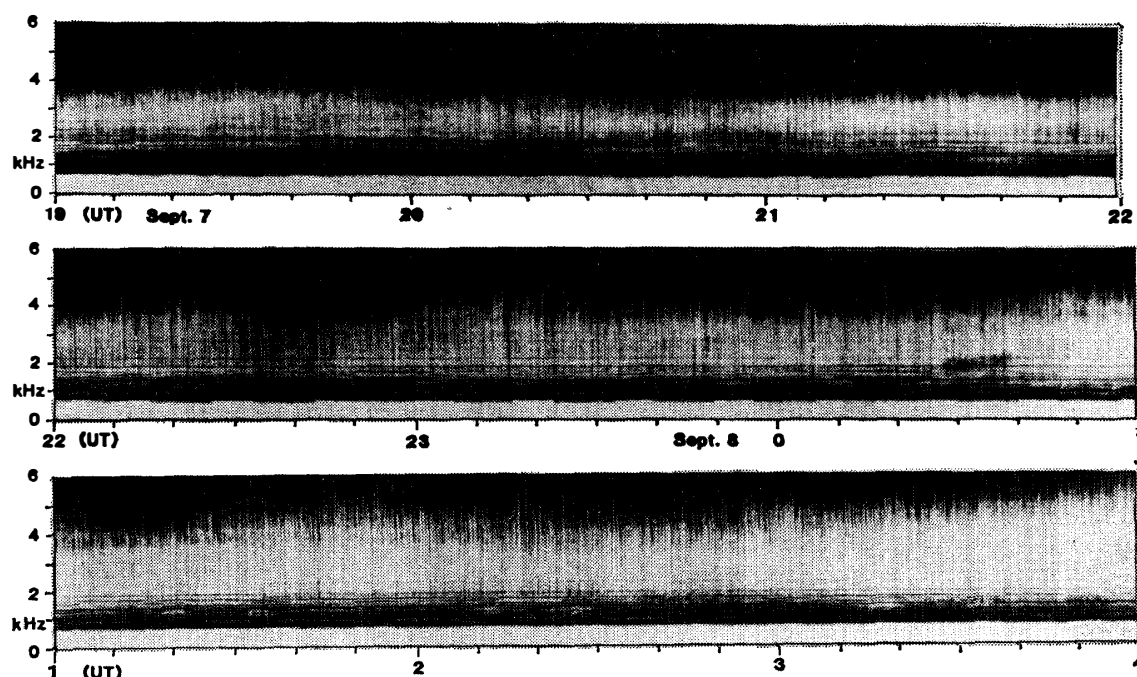

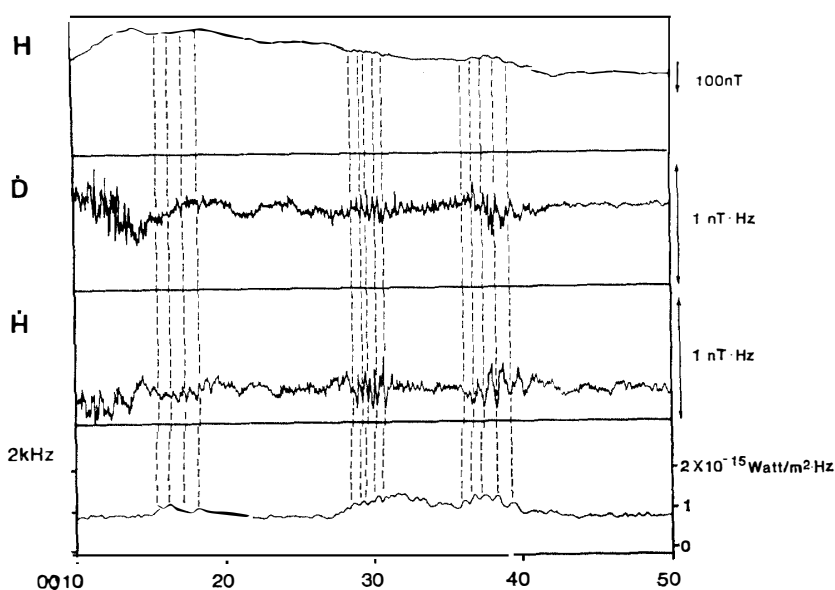Fig. 18.   VLF frequency dynamic spectrum for September 7 event.

Fig. 19.   Correlation between 2 kHz intensity of VLF emissions and geomagnetic pulsations for September 7 event.

over the Esrange.   The corresponding VLF frequency dynamic spectrum is illustrated
in Fig. 18 where intensity increases from white to black.   Although the long time-
scale (tens of minutes) variations of VLF emissions do not follow the changes in geo-
magnetic field, there is good correlation between the short time-scale intensity changes
of VLF emissions and geomagnetic pulsations with a period of 20 s to 60 s.   One
example is shown in Fig. 19 for the recovery phase, 0010 UT to 0050 UT.   As is evident
from the figure, the intensity variations of 2 kHz VLF emissions are mostly anticor-
related with the H-component of pulsations.   An enlarged VLF frequency dynamic
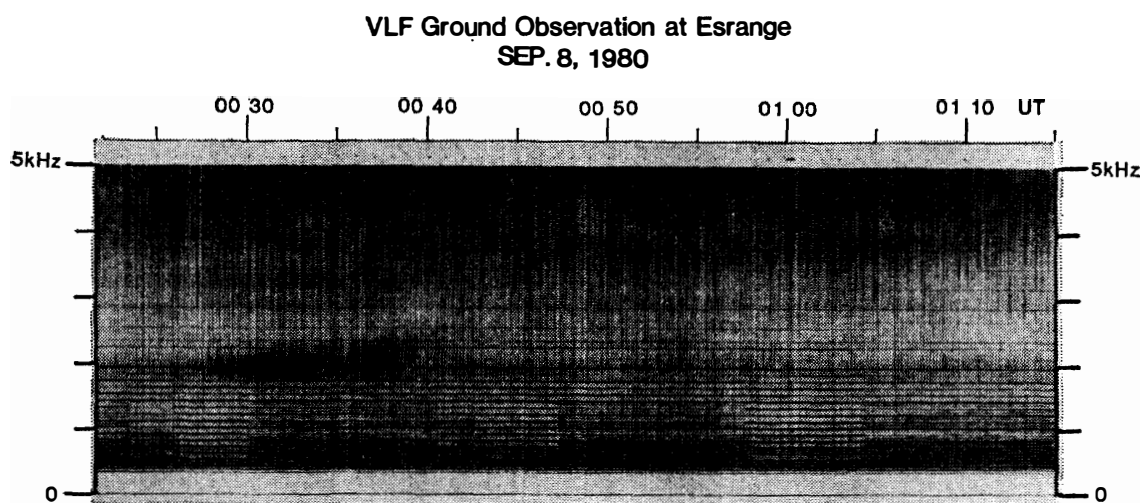spectrum for these emissions is shown in Fig. 20 for reference.

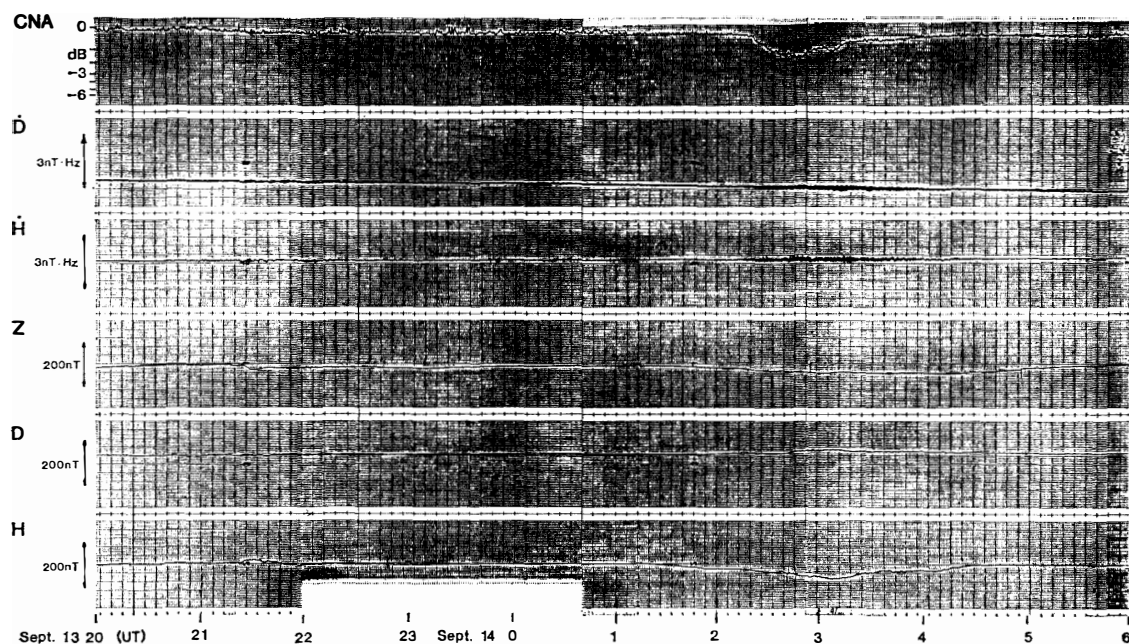*Fig. 20.   VLF frequency dynamic spectrum for the period from 0020 UT to 0110 UT.*

Fig. 21.   September 13 event; ground-based observations.

3.4.2. September 13 event

Figure 21 illustrates the observed data of CNA (cosmic noise absorption), geomagnetic pulsations and 3-components of geomagnetic field for the period of September 13, 20 UT to September 14, 06 UT; A 20 nT positive bay appeared on September 13,
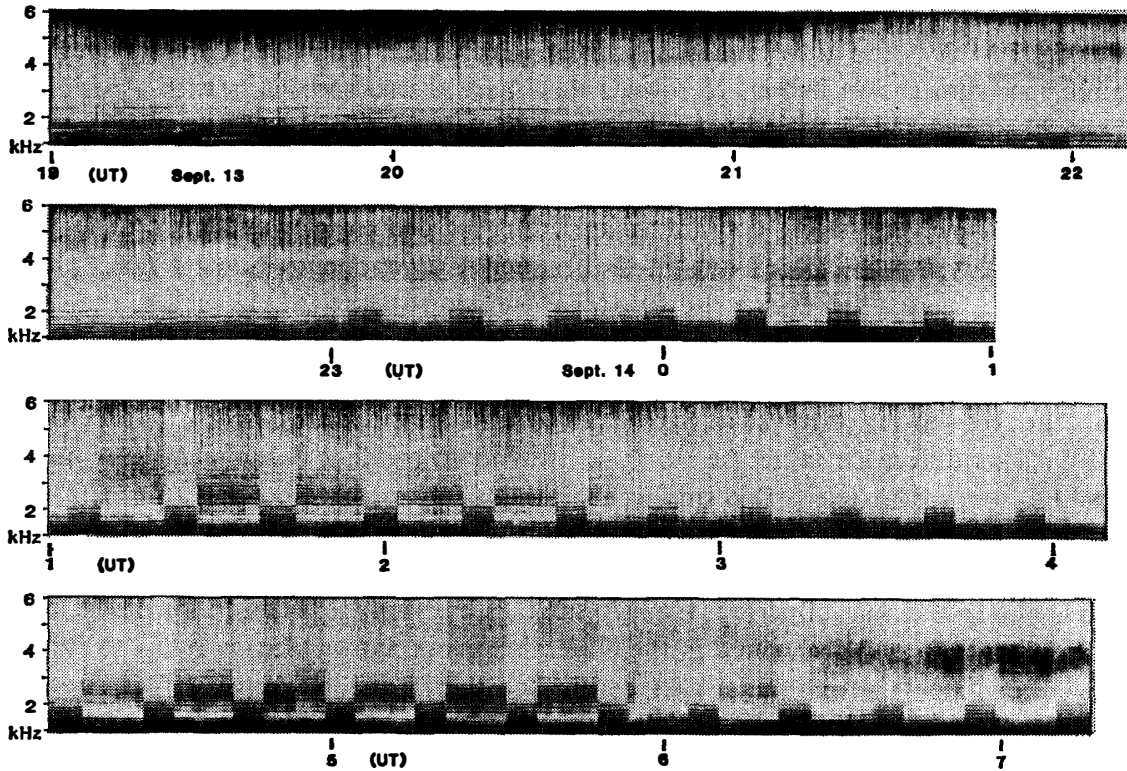
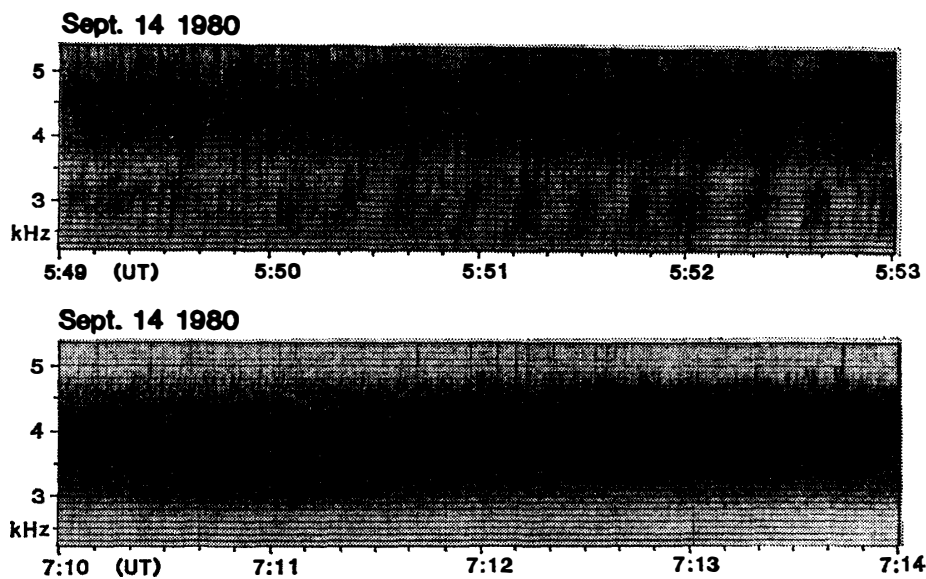Fig. 22. VLF frequency dynamic spectrum for September 13 event.

Fig. 23. Time-enlarged segments of examples of structured (upper panel) and non-structured (lower panel) VLF emissions.

at 2130 UT, and 60 nT negative bay with 1.5 dB CNA indicates a small geomagnetic substorm. The corresponding frequency spectrum of observed VLF emissions is illustrated in Fig. 22, and is different from the previous event. Note that the spectrum was contaminated strongly by the ground power line harmonics which came on and off due to the thermostat operation in the buildings. Up to September 14, 05 UT there is wide band VLF hiss around 3 kHz to 4 kHz with low intensity, and thereafter the intensity increase and the frequency tends to decrease. The detailed frequency dynamic spectrum shown in Fig. 23 reveals that there is structured hiss with a period of about 20 s from 05 UT to 0630 UT, and thereafter nonstructured hiss.

3.4.3.   Comparisons with Antarctic observations

Since there was strong contamination from the ground power lines on the VLF data, no analysis was carried out on the frequency components below 1 kHz. Even though there were a few events showing VLF emissions below 2 kHz such as the dawn chorus observed on September 12 (not presented in this paper), most of the VLF emissions observed at Esrange are in the frequency range around or above 2 kHz to 3 kHz, while the frequencies observed at Syowa Station, Antarctica range below 2 kHz (SATO, 1980). This difference might be partly attributed to the fact that the L-value at Esrange (L=approximately 5.5) is smaller than that at Syowa Station (L=approximately 6.2).

Good correlation of short time-scale changes in intensity of VLF emissions with geomagnetic pulsations of periods from 20 s to 60 s, previously discussed for the September 7 event, were also discovered in the QP emissions at Syowa Station by SATO (1980). These show the same characteristics except for the frequency range. This suggests considering the generation mechanism of VLF-ELF emissions observed both at Esrange and at Syowa. The structured VLF emissions observed between 0500 UT and 0630 UT on September 14 are very similar to the QP emissions, but there is a large frequency difference between them.

4.   Conclusions

The first Japanese balloon campaign at a northern high-latitude has been carried out at Esrange, Kiruna. Measuring systems for X-rays, ozone, atmospheric temperature and pressure, VLF waves and technological balloon flight techniques have been established in this campaign. Since the geomagnetic conditions for both flights did not encounter a polar disturbance condition due to the limited campaign period (launching window), no substorm associated phenomena were observed. On the contrary, the basic data of height profiles of X-ray intensities, ozone density, atmospheric temperature and pressure, corresponding to the quiet magnetic conditions at the high-latitude, were obtained.

As for X-ray observations, these first two flights were carried out with the simplest design of payload and succeeded in obtaining a satisfactory intensity-altitude profile. Further observations using a directional telescope type of payload will follow in a future balloon campaign.

Ozone density together with atmospheric temperature and pressure is one of basic

physical quantities in the stratosphere. It is also important to measure these quantities along with NOx, HOx, and ClOx. For the next balloon campaigns at northern (Norway and Sweden) and southern (Syowa Station) high-latitudes it is planned to measure the NO_2 density simultaneously at both places.

VLF wave propagation between the lower ionosphere and the ground in the wave-guide mode and characteristics of higher harmonics of power line radiations should be investigated quantitatively in the next campaign, as well as VLF emissions associated with auroral activities.

Ground-based observations revealed the characteristics of VLF emissions to be different from those observed at Syowa Station. It is recognized that simultaneous observations at the high-latitudes of both hemispheres are essential in order to understand the generation mechanisms of VLF emissions and also to justify a balloon experiment.

Acknowledgments

References

AYUKAWA, M. and EJIRI, M. (1981): Nihon-Sueden kokusai kyôdô daikikyû kansoku hôkoku (Japanese-Swedish first balloon experiment). Nankyoku Shiryô (Antarct. Rec.), 72, 84–100.

BARCUS, J. R., BROWN, R. R., KARAS, R. H., BRONSTAD, K., TREFALL, H., KODAMA, M. and ROSENBERG, T. J. (1973): Balloon observations of auroral-zone X-rays conjugate regions. J. Atmos. Terr. Phys., 35, 497–511.

CHANDRA, S. and MAEDA, K. (1980): A search for correlation between geomagnetic activity and stratospheric ozone. Geophys. Res. Lett., 7, 757–760.

HILSENRATH, E. (1980): Rocket observations of the vertical distribution of ozone in the polar night and during a mid-winter stratospheric warming. Geophys. Res. Lett., 7, 581–584.

HILSENRATH, E., HEATH, D. F. and SCHLESINGER, B. M. (1979): Seasonal and interannual variation in total ozone revealed by the Nimbus 4 backscattered ultraviolet experiment. J. Geophys. Res., 84, 6969–6979.

IMHOF, W. L., KILNER, J. R., NAKANO, G. H. and REAGAN, J. B. (1980): Satellite X-ray mappings of sporadic auroral zone electron precipitation events in the local dusk sector. J. Geophys. Res., 85, 3347–3359.

KOBAYASHI, J. and TOYAMA, Y. (1966): On various methods of measuring the vertical distribution of atmospheric ozone (III). Pap. Meteorol. Geophys., 17, 113–126.

KODAMA, M., OGURA, K., TAMAI, E. and OGUTI, T. (1972): Nankyoku Syowa Kiti ni okeru ôrora X-sen no kikyû kansoku (Balloon observations of auroral X-rays at Syowa Station,

Antarctica). Rep. Inst. Phys. Chem. Res., **48** (6), 145–165.

MAUK, B. H., CHIN, J. and PARKS, G. (1981): Auroral X-ray images. J. Geophys. Res., **86**, 6827–6835.

NICOLET, M. (1975): On the production of nitric oxide by cosmic rays in the mesosphere and stratosphere. Planet. Space Sci., **23**, 637–649.

PETERSON, L. E. (1969): Properties of individual X-ray sources. Non solar X- and gamma-ray astronomy. IAU Symp., **37**, 59–80.

ROSENBERG, T. J., SIREN, J. C., MATTHEWS, D. L., MARTHINSEN, K., HOLTET, J. A., EGELAND, A., CARPENTER, D. L. and HELLIWELL, R. A. (1981): Conjugacy of electron microbursts and VLF chorus. J. Geophys. Res., **86**, 5819–5832.

SATO, N. (1980): Quasi-Periodic (QP) ELF-VLF emissions observed in high latitudes. Mem. Natl Inst. Polar Res., Ser. A, **17**, 1–120.

WAIT, J. R. (1962): Electromagnetic Waves in Stratified Media. New York, Pergamon, 132–193.

WINCKLER, J. R., PETERSON, L., ARNOLDY, R. and HOFFMAN, R. (1958): X-rays from visible aurorae at Minneapolis. Phys. Rev., **110**, 1221–1231.

YAMAGAMI, T., FUJI, M., NISHIMURA, J., MURAKAMI, H., HIRASIMA, Y., KAJIWARA, M., OKUDAIRA, K. and KODAMA, M. (1978): Balloon observations of auroral X-ray in Canada. I. Determination of auroral X-ray illuminating regions. J. Geomagn. Geoelectr., **30**, 663–682.